Appl. Phys. B 91, 499–505 (2008)
DOI: 10.1007/s00340-008-3001-y

Applied Physics B
Lasers and Optics

X.H. GONG[1,2]
Y.F. LIN[1]
Y.J. CHEN[1]
J.S. LIAO[1]
X.Y. CHEN[1]
Z.D. LUO[1]
Y.D. HUANG[1,✉]

Polarized spectral analysis of Er^{3+} ions in biaxial $Bi_2(MoO_4)_3$ crystal

[1] National Engineering Research Center for Optoelectronic Crystalline Materials, Fujian Institute of Research on the Structure of Matter, Chinese Academy of Sciences, Fuzhou, Fujian 350002, P.R. China
[2] Graduate School of the Chinese Academy of Sciences, Beijing 100039, P.R. China

Received: 16 October 2007 / Revised version: 15 January 2008
Published online: 25 April 2008 • © Springer-Verlag 2008

ABSTRACT An Er^{3+}:$Bi_2(MoO_4)_3$ single crystal has been grown by the Czochralski technique. The Stark sublevels of the $^4I_{15/2}$ and $^4I_{13/2}$ multiplets of Er^{3+} ions in the crystal were determined. The polarized absorption spectra, polarized fluorescence spectra, and fluorescence decay curve of the crystal were measured at room temperature and the relevant spectroscopic parameters, including the Judd–Ofelt intensity parameters, spontaneous emission probability, fluorescence branching ratio, radiative lifetime, and stimulated emission cross section, were estimated. The effect of re-absorption on the spectroscopic parameters was discussed. When the crystal was excited at 977 nm, up-conversion green fluorescence was observed and discussed.

PACS 78.20-e; 42.70.Hj

1 Introduction

Er^{3+} is a well-known active ion for a solid-state laser in the infrared and visible ranges. In recent years, much attention has been devoted to the research of the Er^{3+}-doped laser materials mainly because its emission around 1.5 μm is eye-safe and matches the so-called third telecommunication window very well [1–3].

$Bi_2(MoO_4)_3$ (hereafter denoted as BM) crystal belongs to the monoclinic system with space group $P2_1/c$ and the cell constants are: $a = 7.685(6)$ Å, $b = 11.491(16)$ Å, $c = 11.929(10)$ Å, $\beta = 115.04(2)°$, $Z = 4$, and $d = 6.26$ g/cm^3 [4, 5]. In this crystal, there are two different crystallographic sites for Bi^{3+} ions [4, 5], which make the rare earth ions doped in the crystal have inhomogeneous broadening in their spectra [6]. Furthermore, since the symmetric vibrations of the Mo–O band in the $(MoO_4)^{2-}$ group are strongly Raman active, the BM crystal may be a potential material for stimulated Raman scattering (SRS) lasers [7].

In this work, an Er^{3+}-doped BM crystal has been grown by the Czochralski method. The Stark sublevels of the $^4I_{15/2}$ and $^4I_{13/2}$ multiplets of Er^{3+} ions in the crystal were determined by the low temperature up-conversion fluorescence spectra. The polarized absorption spectra, polarized fluorescence spectra, and fluorescence decay curve of the crystal were measured at room temperature. Based on the Judd–Ofelt (J–O) theory [8, 9], reciprocity method [10], and Fuchtbauer–Landenburg (F–L) formula [11], the relevant spectroscopic parameters were estimated and analyzed. The effect of re-absorption on the spectroscopic parameters was also discussed. Furthermore, when the crystal was excited at 979 nm at room temperature, up-conversion green fluorescence was observed and discussed.

✉ Fax: +86-591-83714946, E-mail: huyd@fjirsm.ac.cn

2 Experimental procedure

An Er^{3+}:BM crystal was grown by the Czochralski method in air using a platinum crucible heated by a 2 kHz radio frequency furnace. In the experiment, the raw materials of Er^{3+}:BM synthesized by solid-state reaction had been heated at a temperature of about 50 °C higher than the melting point for 2 h to melt homogeneously. The crystal was grown at a pulling rate of 0.5–1 mm/h and a rotating rate of 15–20 r/min. After the growth, the crystal was drawn above the surface of the melt and cooled down to room temperature at a rate of −10 °C/h.

The concentration of Er^{3+} ions in the grown crystal was measured to be 0.77 at. % (6.502×10^{19} ions/cm^3) by the inductively coupled plasma atomic emission spectrometer method. Taking the 1.0 at. % Er^{3+} concentration in the initial melt into account, the segregation coefficient of Er^{3+} in the BM single crystal was calculated to be 0.77.

The three optical indicatrix axes of Er^{3+}:BM crystal was determined by means of the X-ray diffraction and polarized microscopy and labeled as X, Y, and Z (the corresponding refractive indices $n_X < n_Y < n_Z$). A high optical quality cuboid sample ($2.92 \times 3.22 \times 4.18$ mm^3) was cut from the grown Er^{3+}:BM crystal with each face perpendicular to one of the optical indicatrix axes. All the faces of the cuboid were optically polished.

The Stark sublevels of the $^4I_{15/2}$ and $^4I_{13/2}$ multiplets of Er^{3+} ions in the crystal were determined by the 5.6 K up-conversion fluorescence spectra. In the experiment, the sample has been cooled to 5.6 K using a He close cycled cryostate. To distinguish the Er^{3+} ions substituting the two different Bi^{3+} crystallographic sites, the exciting wavelengths provided by a Ti:sapphire tunable laser were carefully selected at 791.4

and 795.1 nm, corresponding to the $^4I_{15/2} \rightarrow {}^4I_{9/2}$ transition of Er^{3+} ions. Under excitation at the same wavelength, the excited Er^{3+} ions could further transit to the $^2H_{9/2}$ multiplet (see Fig. 1a). The up-conversion fluorescence spectra in the ranges of 540–580 nm and 840–900 nm, corresponding to the $^4S_{3/2} \rightarrow {}^4I_{15/2}$ and $^4S_{3/2} \rightarrow {}^4I_{13/2}$ transitions respectively, were recorded by a spectrophotometer (1000M, Spex) with an InGaAs detector (IGA020TC, Jobin-Yvon).

The room temperature (RT) absorption spectra in a range of 400–1700 nm were recorded using the Perkin Elmer UV-VIS-NIR Spectrometer (Lambda–900) with the polarization of the incident light parallel to the X, Y, and Z axes of the crystal, respectively. The RT fluorescence spectra in a range from 1400 to 1700 nm with polarizations of the emission light along the optical indicatrix axes were recorded using a spectrophotometer (FL920, Edinburgh) when the sample was excited by a Xe-lamp at 979 nm. The fluorescence signals were detected with an NIR PMT (R5509, Hamamatsu). The fluorescence decay curves at wavelengths of 1535 and 980 nm, corresponding to the transitions of $^4I_{13/2} \rightarrow {}^4I_{15/2}$ and $^4I_{11/2} \rightarrow {}^4I_{15/2}$, respectively, were recorded by the same spectrophotometer when a microsecond flash lamp (μF900, Edinburgh) was used as the exciting source and the exciting wavelengths were 979 and 523 nm, respectively. Furthermore, excited at 979 nm by a diode laser, the room temperature polarized up-conversion fluorescence signals past a monochromator (Triax550, Jobin-Yvon) were detected with a PMT (R928, Hamamasu).

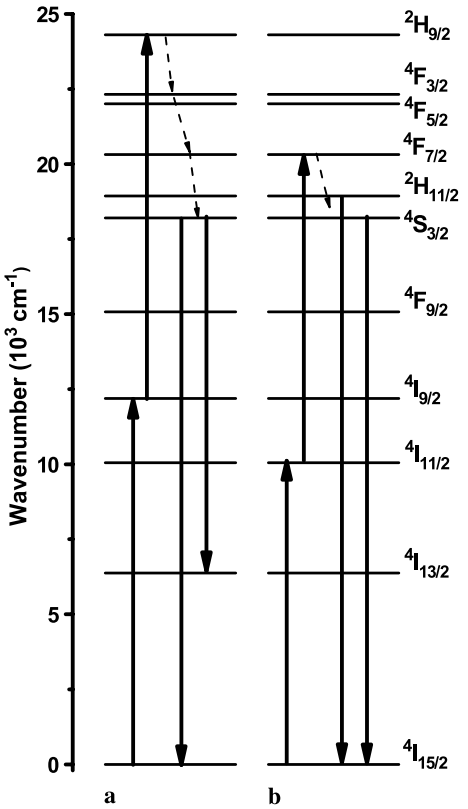

FIGURE 1 Energy level diagram of Er^{3+} ions involved in up-conversion processes: (**a**) for the up-conversion from the $^4I_{9/2}$ multiplet at 5.6 K while excited at 791.4 and 795.1 nm; (**b**) for the up-conversion from the $^4I_{11/2}$ multiplet at room temperature while excited at 979 nm

3 Results and discussion

3.1 *Absorption spectra and* J–O *analysis*

To characterize the electric-dipole transitions for biaxial crystal, three orientations are needed, i.e., $E \| X$, $E \| Y$, and $E \| Z$. The RT polarized absorption spectra of the Er^{3+}:BM crystal are shown in Fig. 2. Only seven absorption bands of Er^{3+} ions can be distinguished due to the narrow energy band gap of 3.3 eV for the BM host crystal [12].

The obtained RT absorption spectra were analyzed by the J–O theory. The detailed calculation procedure is similar to that reported in [1]. The values of the refractive indices for the three polarizations were taken from [12], and the reduced matrix elements of unit tensor operators used in the calculation could be found in [13, 14]. The measured and calculated oscillator strength, denoted as f_{exp} and f_{cal}, respectively, and the root mean square deviations RMS Δf are listed in Table 1. For the Er^{3+} ion, the magnetic dipole transitions of the $^4I_{15/2} \rightarrow {}^4I_{13/2}$ transition cannot be ignored [14] and the values of f_{md} are also listed in Table 1. The calculated intensity parameters Ω_{t} are listed in Table 2. For the biaxial crystal, the effective intensity parameters are defined as $\Omega_{\text{t}}^{\text{eff}} = (\Omega_{\text{t},X} + \Omega_{\text{t},Y} + \Omega_{\text{t},Z}/3)$ [15]. The three effective phenomenological intensity parameters of Er^{3+}:BM crystal are: $\Omega_2^{\text{eff}} = 7.58 \times 10^{-20}$, $\Omega_4^{\text{eff}} = 1.37 \times 10^{-20}$, and $\Omega_6^{\text{eff}} = 0.91 \times 10^{-20}$ cm^2. On the basis of the calculated intensity parameters, the values of spontaneous emission probability A, fluorescence branching ratio β, and radiative lifetime τ_{r} for the main fluorescence levels of Er^{3+} ions in the crystal could be calculated and the results are listed in Table 3.

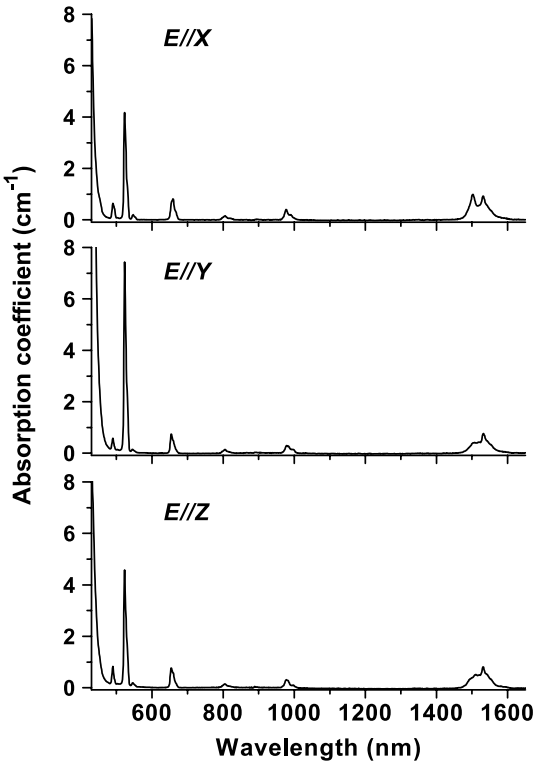

FIGURE 2 Room temperature polarized absorption spectra of the Er^{3+}:BM crystal

J'-multiplet	$\overline{\lambda}_{abs}$ (nm)	f (10^{-6} cm^2) $E\|X$ f_{exp}	$E\|X$ f_{cal}	$E\|Y$ f_{exp}	$E\|Y$ f_{cal}	$E\|Z$ f_{exp}	$E\|Z$ f_{cal}
$^4I_{13/2}$	1525	3.03	2.32 (ed) 0.66 (md)	2.06	1.36 (ed) 0.67 (md)	2.22	1.47 (ed) 0.71 (md)
$^4I_{11/2}$	977	1.00	1.18	0.89	0.94	0.82	0.81
$^4I_{9/2}$	806	0.55	0.57	0.50	0.48	0.64	0.52
$^4F_{9/2}$	655	3.73	3.73	2.62	2.62	2.95	2.96
$^4S_{3/2}$	547	0.74	0.97	0.43	0.48	0.51	0.59
$^2H_{11/2}$	522	17.84	17.83	28.97	28.97	18.58	18.58
$^4F_{7/2}$	490	3.92	4.05	2.13	2.31	2.52	2.82
RMS Δf (10^{-7} cm^2)			1.61		0.97		1.67
RMS error (%)			2.3		0.88		2.3

TABLE 1 Mean wavelength and polarized experimental and calculated oscillator strengths of Er^{3+}:BM crystal

Ω_t (10^{-20} cm^2)	$E\|X$	$E\|Y$	$E\|Z$
Ω_2	6.40	10.80	5.55
Ω_4	1.57	1.30	1.25
Ω_6	1.39	0.66	0.69

TABLE 2 The J–O parameters of Er^{3+}:BM crystal

3.2 *Fluorescence spectra and stimulated emission cross section for $^4I_{13/2} \rightarrow {}^4I_{15/2}$*

The 5.6 K up-conversion fluorescence spectra, corresponding to the $^4S_{3/2} \rightarrow {}^4I_{15/2}$ and $^4S_{3/2} \rightarrow {}^4I_{13/2}$ transitions, are shown in Fig. 3. Sites 1 and 2 in this figure correspond to the exciting wavelengths of 791.4 and 795.1 nm, respectively. The positions of Stark sublevels in the $^4I_{13/2}$ and $^4I_{15/2}$ multiplets of Er^{3+} ions at two sites deduced from the spectra are listed in Table 4. The maximum Stark splittings of both $^4I_{13/2}$ and $^4I_{15/2}$ multiplets for site 1 are larger than those for site 2. In fact, the summations of the Bi-O vectors about two sites of Bi^{3+} ions in BM crystal are about 2.8 and 0.1 Å, respectively [4, 5]. This reveals that one site is more asymmetric, though both sites have the same point symmetry of C_s.

For the important transition channel $^4I_{13/2} \rightarrow {}^4I_{15/2}$ of Er^{3+} laser, the emission cross section at wavelength λ with different polarizations can be derived from the polarized emission spectra by the F-L formula [11]. However, due to the overlap of the absorption spectrum and the emission spectrum of Er^{3+} ions around 1.5 μm, the measured fluorescence spectra are generally distorted by the re-absorption [16, 17]. Furthermore, since the assumption of average population among the Stark levels in a multiplet in the spectral analysis on the basis of the J-O theory is not fully satisfied at room temperature, the calculated spontaneous emission probability may differ from the actual one [18]. The emission cross section calculated by this method would depart from the intrinsic one.

$J' \rightarrow J$		$E\|X$ A (s^{-1})	$E\|X$ β (%)	$E\|Y$ A (s^{-1})	$E\|Y$ β (%)	$E\|Z$ A (s^{-1})	$E\|Z$ β (%)	τ_r (ms)
$^4I_{13/2}$	$^4I_{15/2}$	447.43	100	319.47	100	388.17	100	2.60
$^4I_{11/2}$	$^4I_{13/2}$	79.45	13.8	63.47	13.3	73.37	15.3	1.96
	$^4I_{15/2}$	496.43	86.2	415.0	86.7	406.71	84.7	
$^4I_{9/2}$	$^4I_{11/2}$	5.32	0.9	5.62	0.8	5.91	1	1.85
	$^4I_{13/2}$	146.15	28.2	75.74	15.6	101.10	17.5	
	$^4I_{15/2}$	430.13	70.9	378.98	83.6	471.91	81.5	
$^4F_{9/2}$	$^4I_{9/2}$	22.44	0.5	36.25	0.7	26.97	0.5	0.22
	$^4I_{11/2}$	234.01	5.0	189.1	4.5	192.04	4.1	
	$^4I_{13/2}$	203.51	4.0	193.46	5.1	206.71	4.4	
	$^4I_{15/2}$	4496	90.5	3298	89.7	4293	91	
$^4S_{3/2}$	$^4F_{9/2}$	2.28	≈0	1.17	0.1	1.56	≈0	0.20
	$^4I_{9/2}$	205.58	3	125.20	3.8	162.50	3.4	
	$^4I_{11/2}$	118.85	1.8	63.30	1.9	84.68	1.8	
	$^4I_{13/2}$	1629	25	832.04	24.6	1136	23.8	
	$^4I_{15/2}$	4575	70.2	2352	69.6	3384	71	
$^2H_{11/2}$	$^4S_{3/2}$	0.10	≈0	0.09	≈0	0.78	≈0	0.02
	$^4F_{9/2}$	94.64	0.3	170.34	0.3	111.85	0.3	
	$^4I_{9/2}$	631.49	1.8	568.68	1.6	741.32	1.8	
	$^4I_{11/2}$	409.16	1.1	307.86	0.9	496.89	1.2	
	$^4I_{13/2}$	439.95	1.3	547.54	1.0	470.79	1.1	
	$^4I_{15/2}$	30970	95.4	52710	96.2	39700	95.6	

TABLE 3 Spontaneous emission probabilities A, fluorescence branching ratios β, and radiative lifetime τ_r for Er^{3+}:BM crystal

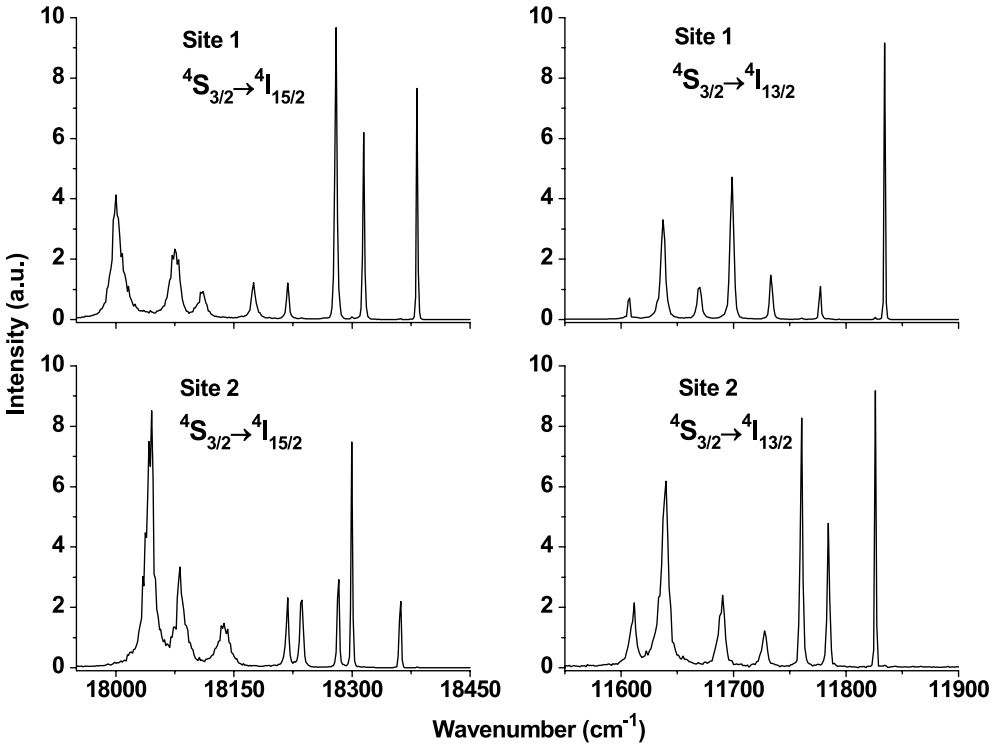

FIGURE 3 5.6 K up-conversion fluorescence spectra of the Er^{3+}:BM crystal when the sample was excited at 791.4 and 795.1 nm, respectively

Multiplet	Stark sublevels (cm^{-1}) Site 1	Site 2
$^4I_{15/2}$	0	0
	67	63
	102	79
	164	126
	207	144
	273	225
	307	281
	382	316
$^4I_{13/2}$	6548	6536
	6605	6578
	6649	6601
	6683	6635
	6712	6672
	6745	6722
	6776	6750

TABLE 4 Stark sublevels for the $^4I_{15/2}$ and $^4I_{13/2}$ multiplets of Er^{3+} ions in BM crystal

The emission cross section can also be calculated by the so-called reciprocity method from the absorption emission cross section by [10, 19]

$$\sigma^{\mathrm{RM}}_{\mathrm{em},q}(\lambda) = \sigma_{\mathrm{abs},q}(\lambda)\exp\left[\frac{\varepsilon - hc/\lambda}{k_{\mathrm{B}}T}\right], \quad (1)$$

where $\sigma^{\mathrm{RM}}_{\mathrm{em},q}$ and $\sigma_{\mathrm{abs},q}$ are the polarized emission and absorption cross section, respectively, h is Planck constant, k_{B} is the Boltzmann constant, and ε is the net free energy required to excite one Er^{3+} ion from the $^4I_{15/2}$ to $^4I_{13/2}$ state at temperature T and can be calculated from the formula proposed in [19]. According to the data listed in Table 4, the calculated values of ε are 6534 and 6528 cm^{-1} for site 1 and site 2, respectively. In our calculation, the average value of 6531 cm^{-1} was adopted. Since the emission cross sections calculated by (1) are from the measured absorption spectra and the Stark splittings of the related multiplets, they can be treated as the intrinsic ones without the influence of re-absorption.

Figure 4 shows the absorption cross section spectra and the emission cross section spectra calculated by the F–L formula and the reciprocity method. It can be seen that, due to the re-absorption effect, the emission cross sections calculated by the F–L formula are smaller in the shorter wavelength region but larger in longer wavelength region compared to those calculated by the reciprocity method. The peak emission cross sections calculated by the reciprocity method are about 1.56×10^{-20}, 1.20×10^{-20}, and $1.26\times10^{-20}\,cm^2$ for $E\|X$, $E\|Y$, and $E\|Z$, respectively, which are comparable to those reported for other Er^{3+}-doped materials, such as 1.1×10^{-20} (π-polarized) and $0.78\times10^{-20}\,cm^2$ (σ-polarized) for Er^{3+}:$NaY(MoO_4)_2$ [20], 0.86×10^{-20} (π-polarized) and $0.95\times10^{-20}\,cm^2$ (σ-polarized) for Ce^{3+}:Er^{3+}:$NaLa(MoO_4)_2$ [21], 2.56×10^{-20} ($E\|X$), 1.65×10^{-20} ($E\|Y$), and $1.26\times10^{-20}\,cm^2$ ($E\|Z$) for Er^{3+}:$KGd(WO_4)_2$ [22], and $0.45\times10^{-20}\,cm^2$ for YAG [23].

Since the Er^{3+} laser via the $^4I_{13/2}\rightarrow{}^4I_{15/2}$ transition operates in a three-level scheme, the possible laser wavelength can be evaluated by the following gain cross section [24]

$$G_q(\lambda) = P\sigma^q_{\mathrm{em}}(\lambda) - (1-P)\sigma^q_{\mathrm{abs}}(\lambda)\,, \quad (2)$$

where P is the population inversion ratio of Er^{3+} ions. The relations between the calculated polarized gain cross section and wavelength with different P values ($P = 0.3$, 0.4, ..., 0.7) are shown in Fig. 5. The smooth and broad gain curves indicate the Er^{3+}:BM is a good candidate for gain medium of tunable and ultra-short lasers and therefore it is also beneficial to the generation of a self-stimulated Raman laser since the

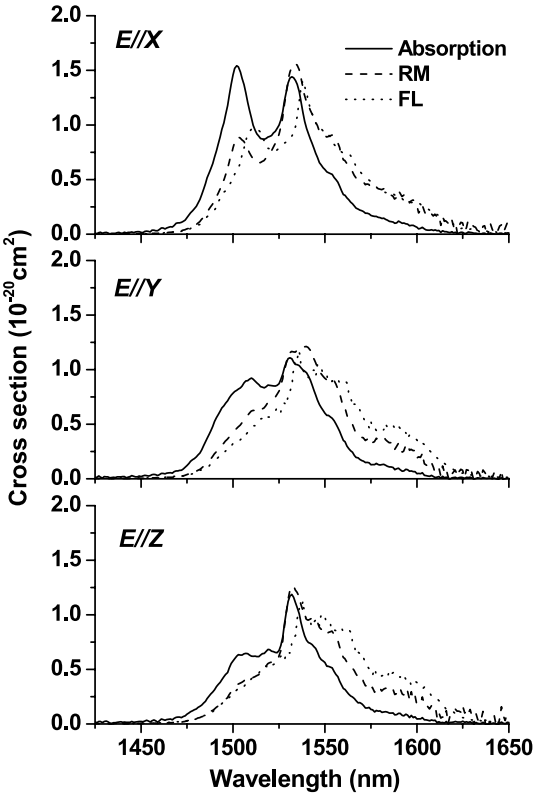

FIGURE 4 Comparison of the polarized absorption and emission cross sections versus wavelength calculated by the reciprocity method and the F–L formula of the Er^{3+}:BM crystal

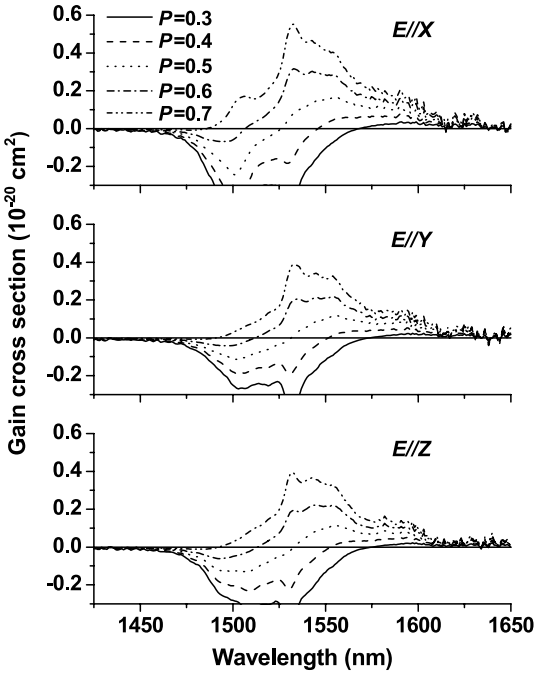

FIGURE 5 Polarized gain cross sections of the Er^{3+}:BM crystal versus wavelength

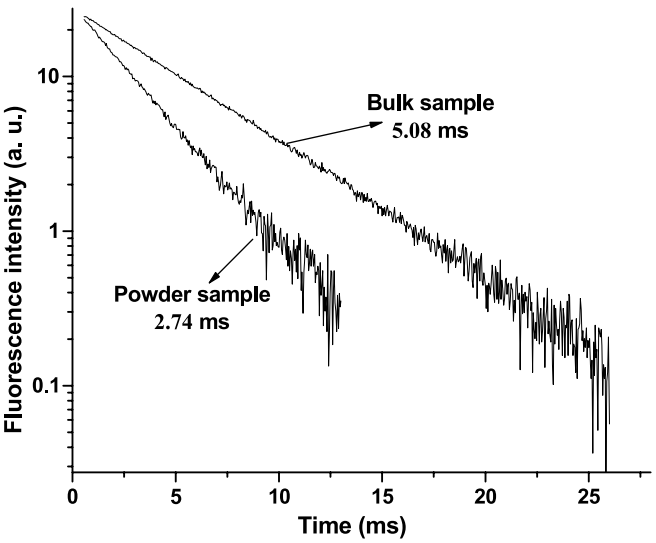

FIGURE 6 Room temperature fluorescence decay curves of the Er^{3+}:BM bulk and powder samples at 1535 nm, the exciting wavelength is 979 nm

Raman gain coefficient is proportional to the intensity of the fundamental laser [25].

3.3 *Fluorescence lifetime and quantum efficiency*

The re-absorption also leads to the increase of the measured fluorescence lifetime [16]. To reduce the influence of the re-absorption on the measured fluorescence lifetime of the $^4I_{13/2}$ multiplet, the powder method was adopted [26]. In our work, the powder was a mixture of 2 wt. % Er^{3+}:BM crystal and 98 wt. % pure BM crystal as dilution with diameter of about 80 μm, and the refractive index matching fluid was monochlorobenzene with refractive index of 1.52. The measured fluorescence decay curves of the powder sample immersed in monochlorobenzene fluid and the bulk crystal sample in air at 1535 nm are shown in Fig. 6 in semilog scale. The linear relationship in the figure displays single exponential behavior of the fluorescence decay and the fluorescence lifetime can be obtained from the slope of the fitting line k, i.e., $\tau_f = -(1/2.303k)$. By linear fitting, the fluorescence lifetimes of the $^4I_{13/2}$ multiplet are about 2.78 and 5.08 ms for the powder and bulk crystal samples, respectively. The large discrepancy between the measured fluorescence lifetimes reveals a strong re-absorption occurred in the bulk sample. In fact, the re-absorption phenomenon has also happened in some other Er^{3+}-doped materials, such as Er^{3+}:$NaY(MoO_4)_2$, Er^{3+}:$LiNbO_3$, and Er^{3+}:KPb_2Br_5 [20, 27, 28].

The fluorescence quantum efficiency of a multiplet is defined as $\eta = \tau_f/\tau_r$. From the values of $\tau_r = 2.60$ ms calculated by the J–O theory and $\tau_f = 2.78$ ms measured in the diluted powder sample, an untrue quantum efficiency larger than one would be deduced. This is mainly caused by the assumption of equal population at the Stark levels in the J–O theory [18]. Since the $^4I_{13/2}$ multiplet of Er^{3+} ions is the first excited state, a more reliable result for the spontaneous emission probability can be obtained from the emission cross sections calculated by the reciprocity method using the F–L formula [11]

$$A_q = \frac{8\pi c n^2 \int \sigma^q_{RM}(\lambda)\,d\lambda}{\int \lambda^4 g_q(\lambda)\,d\lambda}, \tag{3}$$

where $g_q(\lambda)$ is the normalized line shape factor of the calculated emission cross section. From the A_q obtained by this

method, the radiative lifetime of $^4I_{13/2}$, i.e., $\tau_r = 3/(A_X + A_Y + A_Z)$, was calculated to be 2.96 ms. Then, the fluorescence quantum efficiency of $^4I_{13/2}$ multiplet was estimated to be 94%. The high quantum efficiency reveals that the multi-phonon non-radiative transition from the $^4I_{13/2}$ multiplet is weak. This is a result of the large energy separation between the $^4I_{13/2}$ and $^4I_{15/2}$ multiplets (about 6300 cm^{-1}) and the low phonon frequency of the $(MoO_4)^{2-}$ group (about 900 cm^{-1}) [7].

In order to evaluate the relaxation rate from the $^4I_{11/2}$ to the $^4I_{13/2}$ upper laser level, the fluorescence lifetime of the $^4I_{11/2}$ multiplet was measured. The lifetimes measured from both the bulk and powder crystal samples are about 108 μs, which indicates that the effect of re-absorption is weak for the emission from the transition of the $^4I_{11/2} \rightarrow {}^4I_{15/2}$. The lifetime is similar to that of Er^{3+}:YAG (100 μs) [29] but longer than those of Er^{3+}:$Ca_2Al_2SiO_7$ (41 μs) [30], YVO_4 (23 μs) [2], and some phosphate glasses (2–3 μs) [31]. As to be discussed in Sect. 3.4, the longer fluorescence lifetime and higher quantum efficiency (5.5%) of $^4I_{11/2}$ in Er^{3+}:BM are disadvantageous to the population in the upper laser level of $^4I_{13/2}$.

3.4 *Up-conversion fluorescence*

In hosts with low phonon frequency the up-conversion via excited state absorption (ESA) and/or non-radiative energy transfer (ET) becomes more effective and reduces the population in the upper laser level of $^4I_{13/2}$. In Sect. 3.2, the low temperature up-conversion fluorescence spectra have been used to determine the positions of Stark levels in the $^4I_{13/2}$ and $^4I_{15/2}$ multiplets. At room temperature, when the crystal was excited at 979 nm, corresponding to the main pumping channel $^4I_{15/2} \rightarrow {}^4I_{11/2}$ for Er^{3+} ions, the polarized up-conversion fluorescence spectra in a range from 500 to 580 nm were recorded and are shown in Fig. 7. The energy level diagram of Er^{3+} ions in Fig. 1b shows that the Er^{3+} ions at the $^4I_{11/2}$ multiplet are further excited to the $^4F_{7/2}$ multiplet and these two up-conversion fluorescence bands correspond to the $^2H_{11/2} \rightarrow {}^4I_{15/2}$ and $^4S_{3/2} \rightarrow {}^4I_{15/2}$ transitions, respectively. To overcome the influence of the up-conversion on the population in the upper laser level $^4I_{13/2}$ when a diode laser at ∼ 970 nm is used as the pumping source, Ce^{3+} ions are generally introduced as deactivators to make the Er^{3+} ions at the $^4I_{11/2}$ multiplet relax to the $^4I_{13/2}$ multiplet faster [21, 32, 33]. For example, the co-doping of Ce^{3+} ions in the Yb^{3+}:Er^{3+}:$Ca_2Al_2SiO_7$ crystal makes the threshold lower and the slope efficiency higher in 1.5 μm laser operation [33]. The BM crystal can be highly doped with Ce^{3+} ions [5] and so efficient 1.5 μm laser emission can be expected in the Ce^{3+} and Er^{3+} co-doped BM crystal and this work is in progress in our lab.

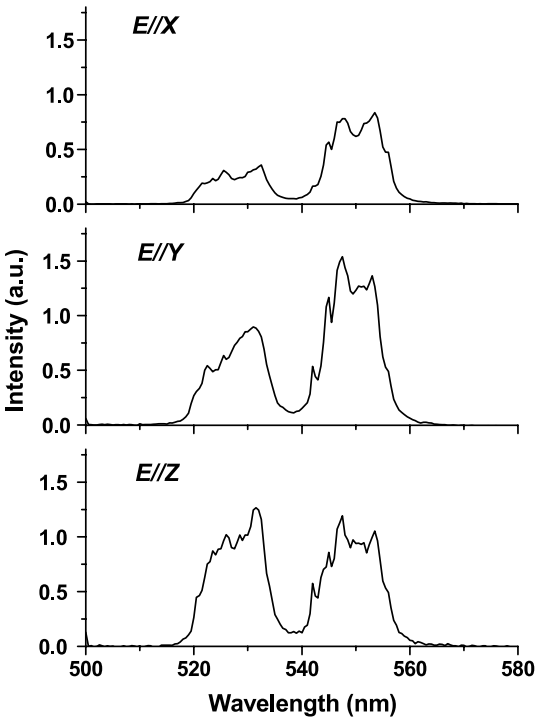

FIGURE 7 Room temperature polarized up-conversion fluorescence spectra of the Er^{3+}:BM crystal under excitation at 979 nm

4 Conclusion

An Er^{3+}:BM crystal has been grown by the Czochralski method. In the framework of the J–O theory, the spectroscopic parameters were calculated. On the basis of the F–L formula and reciprocity method, the effect of re-absorption on the fluorescence spectra of the $^4I_{13/2} \rightarrow {}^4I_{15/2}$ transition was discussed and the peak stimulated emission cross sections of the transitions were estimated. The gain cross section curves of the $^4I_{13/2} \rightarrow {}^4I_{15/2}$ transition were also provided and discussed. At last, the powder method was used to eliminate the effect of re-absorption on the fluorescence lifetime and the fluorescence quantum efficiency was estimated to be 94%. The main spectroscopic parameters of some Er^{3+}-doped

Crystals	Ω_t (10^{-20} cm^2)			λ_{em} (nm)	σ_{em} (10^{-20} cm^2)	τ_r (ms)	Ref.
	Ω_2	Ω_4	Ω_6				
$Bi_2(MoO_4)_3$	7.58	1.37	0.91	1532	1.56 ($E\|\|X$) 1.20 ($E\|\|Y$) 1.26 ($E\|\|X$)	2.60	This work
$KGd(WO_4)_2$	8.90	0.96	0.82	1548	2.56 ($E\|\|X$) 0.17 ($E\|\|Y$) 1.26 ($E\|\|Z$)	5.99	[1, 22]
$Ca_2Al_2SiO_7$	3.85	1.85	1.0	1535	0.8	6.80	[30, 33]
YAG	0.45	0.98	0.62	1550	0.45	4.06	[23, 34]
YVO_4	13.45	2.23	1.67	1550	1.0	2.30	[35, 36]

TABLE 5 Comparison of the spectroscopic parameters of some Er^{3+}-doped laser crystals

crystals listed in Table 5 reveal that the spectroscopic parameters of Er^{3+}:BM crystal are comparable to those of other Er^{3+}-doped crystals, in which laser action around 1.5 μm have been demonstrated while Yb^{3+} ions are co-doped as the sensitizer [33, 36–38]. All of the above results indicate that the Er^{3+}-doped or Er^{3+}/Yb^{3+}-co-doped $Bi_2(MoO_4)_3$ crystal may be a candidate for gain medium of tunable and ultrashort lasers, and furthermore, for a self-stimulated Raman laser when the Raman active of $Bi_2(MoO_4)_3$ is taken into account.

ACKNOWLEDGEMENTS This work has been supported by the National Natural Science Foundation of China (grants 60778015 and 50590405), the Major Program of Science and Technology Foundation of Fujian Province (grant 2005HZ1024), and the Natural Science Foundation of Fujian Province (grant A0610031).

REFERENCES

1 M.C. Pujol, M. Rico, C. Zaldo, R. Sole, V. Nikolov, X. Solans, M. Augilo, F. Diaz, Appl. Phys. B **68**, 187 (1998)
2 N.A. Tolstik, A.E. Troshin, S.V. Kurilchik, V.E. Kisel, N.V. Kuleshov, V.N. Matrosov, T.A. Matrosova, M.I. Kupchenko, Appl. Phys. B **86**, 275 (2007)
3 A.A. Kaminskii, V.S. Mironov, A. Kornienko, S.N. Bagaev, G. Boulon, A. Brenier, B.D. Bartolo, Phys. Stat. Solidi A **151**, 231 (1995)
4 A.F. van den Elzen, G.D. Rieck, Acta Cryst. B **29**, 2433 (1973)
5 R.G. Teller, J.F. Brazdil, R.K. Grasselli, J. Solid State Chem. **52**, 313 (1984)
6 M. Montes, C. de las Heras, D. Jaque, Opt. Mater. **28**, 408 (2006)
7 B. Mihailova, G. Bogachev, M. Gospodinov, L. Konstantinov, J. Raman Spectrosc. **30**, 195 (1999)
8 B.R. Judd, Phys. Rev. **127**, 750 (1962)
9 G.S. Ofelt, J. Chem. Phys. **37**, 511 (1962)
10 D.E. McCumber, Phys. Rev. A **136**, 954 (1964)
11 B.F. Aull, H.P. Jenssen, IEEE J. Quantum Electron. **QE-18**, 925 (1982)
12 V. Marinova, M. Veleva, Opt. Mater. **19**, 329 (2002)
13 M.J. Weber, Phys. Rev. **157**, 262 (1967)
14 W.T. Carnall, P.R. Fields, K. Rajnak, J. Chem. Phys. **49**, 4424 (1968)
15 Z. Luo, X. Chen, T. Zhao, Opt. Commun. **134**, 415 (1997)
16 D.S. Sumida, T.Y. Fan, Opt. Lett. **19**, 1343 (1994)
17 Y.J. Chen, X.Q. Lin, Z. Luo, Y.D. Huang, Opt. Mater. **27**, 625 (2004)
18 F. Auzel, J. Alloys Compd. **380**, 9 (2003)
19 W.J. Miniscalco, R.S. Quimby, Opt. Lett. **16**, 258 (1994)
20 X.A. Lu, Z.Y. You, J.F. Li, Z.J. Zhu, G.H. Jia, B.C. Wu, C.Y. Tu, J. Alloys Compd. **426**, 352 (2006)
21 E. Sani, A. Toncelli, M. Tonelli, J. Appl. Phys. **97**, 123 531 (2000)
22 X. Mateos, M.C. Pujol, F. Guell, M. Galan, R.M. Sole, J. Gavalda, M. Gaulio, J. Massons, F. Diaz, IEEE J. Quantum Electron. **QE-40**, 759 (2004)
23 S.A. Payne, L.L. Chase, L.K. Smith, L. Kway, W.F. Krupke, IEEE J. Quantum Electron. **QE-28**, 2619 (1992)
24 K. Ohta, H. Saito, M. Obara, J. Appl. Phys. **73**, 3149 (1993)
25 W. Koechner, *Solid-State Laser Engineering* (Springer, Berlin Heidelberg New York, 1992)
26 M.C. Pujol, M.A. Bursukova, F. Guell, X. Mateos, R. Sole, J. Gavalda, M. Aguilo, J. Massons, F. Diaz, P. Klopp, U. Griebner, V. Petrov, Phys. Rev. B **65**, 165 121 (2002)
27 J. Amin, B. Dussardier, T. Schweizer, M. Hempstead, J. Luminesc. **69**, 17 (1996)
28 U. Hommerich, E.E. Nyein, S.B. Trivedi, J. Luminesc. **113**, 100 (2005)
29 T. Schweizer, T. Jensen, E. Heumann, G. Huber, Opt. Commun. **118**, 557 (1995)
30 B. Simondi-Teisseire, B. Viana, D. Vivien, A.M. Lejus, Phys. Stat. Solidi A **155**, 249 (1996)
31 G. Karlsson, F. Laurel, J. Tellefsen, B. Denker, B. Galagan, V. Osiko, S. Sverchkov, Appl. Phys. B **75**, 41 (2002)
32 J. Xu, L.B. Su, H.J. Li, L. Wen, H. Lin, G.J. Zhao, Opt. Mater. **29**, 932 (2007)
33 B. Simondi-Teisseire, B. Viana, A.M. Lejus, J.-M. Benitez, D. Vivien, C. Borel, R. Templier, C. Wyon, IEEE J. Quantum Electron. **QE-32**, 2004 (1996)
34 A.A. Kaminskii, A.G. Petrosyan, G.A. Denisenko, T.I. Butaeva, V.A. Fedorov, S.E. Sarkisov, Phys. Stat. Solidi A **71**, 291 (1982)
35 J.A. Capobianco, P. Kabro, F.S. Ermeneux, R. Moncorge, M. Bettinelli, E. Cavalli, Chem. Phys. **214**, 329 (1997)
36 I. Sokolska, E. Heumann, S. Kuck, T. Lukasiewicz, Appl. Phys. B **71**, 893 (2000)
37 Y.E. Young, S.D. Setzler, K.J. Snell, P.A. Budni, T.M. Pollak, E.P. Chicklis, Opt. Lett. **29**, 1075 (2004)
38 N.V. Kuleshov, A.A. Lagatsky, V.G. Shcherbitsky, V.P. Mikhailov, E. Heumann, T. Jensen, A. Diening, G. Huber, Appl. Phys. B **64**, 409 (1997)